

ISSLS Prize Winner: Microstructure and Mechanical Disruption of the Lumbar Disc Annulus

Part II: How the Annulus Fails Under Hydrostatic Pressure

Samuel P. Veres, BEng,* Peter A. Robertson, MD,† and Neil D. Broom, PhD*

Study Design. Mechanically induced annular disruption of lumbar intervertebral discs followed by microstructural investigation.

Objective. To investigate the role that elevated nuclear pressures play in disrupting the lumbar intervertebral disc's annulus fibrosus.

Summary of Background Data. Compound mechanical loadings have been used to recreate clinically relevant annular disruptions *in vitro*. However, the role that individual loading parameters play in disrupting the lumbar disc's annulus remains unclear.

Methods. The nuclei of ovine lumbar intervertebral discs were gradually pressurized by injecting a viscous radio-opaque gel *via* their inferior vertebrae. Pressurization was conducted until catastrophic failure of the disc occurred. Investigation of the resulting annular disruption was carried out using microcomputed tomography and differential interference contrast microscopy.

Results. Gel extrusion from the posterior annulus was the most common mode of disc failure. Unlike other aspects of the annular wall, the posterior region was unable to distribute hydrostatic pressures circumferentially. In each extrusion case, severe disruption of the posterior annulus occurred. Although intralamellar disruption occurred in the mid annulus, interlamellar disruption occurred in the outer posterior annulus. Radial ruptures between lamellae always occurred in the mid-axial plane.

Conclusion. With respect to the annular wall, the posterior region is most susceptible to failure in the presence of high nuclear pressure, even when loaded in the neutral position. Weak interlamellar cohesion of the outer posterior lamellae may explain why the majority of herniations remain contained as protrusions within the outer annular wall.

Key words: nuclear pressurization, disc herniation, annular disruption, differential interference contrast microscopy, micro-computed tomography. **Spine 2008;33:2711–2720**

The outer annular wall of the lumbar disc is known to be innervated,^{1–3} and stimulation by mechanical probing has shown to elicit pain in the lower back.⁴ Radial tears

that extend from the nucleus into the outer third of the annulus readily reproduce a patient's symptomatic low back pain on discography.^{5–7} Such tears, which are classified by Aprill and Bogduk⁵ as grade 3 or 4 manifestations of internal disc disruption,⁸ may account for 30% to 50% of chronic low back pain cases.⁹

Disc herniation, defined as the migration of nuclear material down an annular fissure causing a distinct localized change to the outer annular wall,¹⁰ may be related to internal disc disruption.¹¹ Although intervertebral disc herniations in the form of protrusions are commonly found in asymptomatic individuals,^{12–14} extrusions and sequestrations correlate well with low back pain and sciatica.^{15,16}

Genetic factors have been shown to play a significant role in the development of lumbar disc degeneration¹⁷ and the occurrence of herniation¹⁸; however, the way in which these factors may weaken the disc structure, predisposing it to structural failure, remains unknown. Several studies have shown an increased risk of disc herniation^{15,19,20} and low back pain^{21,22} among persons exposed to adverse mechanical factors. In an attempt to pinpoint the specific loading combinations that make up these mechanical risk factors, numerous studies have sought to create annular tears or herniation *in vitro*.^{23–32} The combined results of these studies demonstrate that compression, flexion/extension, and axial rotation of the spine may all play some role in the development of these 2 conditions.

High-resolution Nomarski differential interference contrast (DIC) microscopy, combined with simultaneous micromechanical testing, has recently documented previously unknown levels of complex structural interconnectivity that exist both within and between the collagenous lamellae of the annulus.^{33,34} Despite the extensive mechanical testing, which has been done to elucidate the loadings that may contribute to annular tearing and disc herniation, the way in which individual loading parameters disrupt the highly connected annular wall remains largely unknown. This gap in the current literature likely exists because obtaining such information is highly problematic. Although magnetic resonance imaging and discography can, at relatively low resolution, describe the three-dimensional (3D) nature of these disruptions, they cannot relate them to the annular architecture. Microscopy, on the other hand, can provide highly detailed structural information, but using two-dimensional tissue sections in order to study 3D disruptions of unknown

From the *Department of Chemical and Materials Engineering, University of Auckland; and †Department of Orthopaedic Surgery, Auckland Hospital, Auckland, New Zealand.

Acknowledgment date: October 12, 2007. First revision date: January 22, 2008. Acceptance date: January 28, 2008.

The manuscript submitted does not contain information about medical device(s)/drug(s).

Corporate/industry and Foundation funds were received in support of this work. No benefits in any form have been or will be received from a commercial party related directly or indirectly to the subject of this manuscript.

Address correspondence and reprint requests to Neil D. Broom, PhD, Department of Chemical and Materials Engineering, University of Auckland, Auckland, New Zealand; E-mail: nd.broom@auckland.ac.nz

extent or location requires time-consuming serial sectioning, as recently demonstrated.³⁵

To begin filling this gap in the current literature, a series of detailed investigations into how compression, flexion/extension, and axial rotation each contribute to disruption of the complex annular architecture is required. Using the recently described technique of nuclear pressurization,³⁶ and by employing a combination of 3D microcomputed tomography (micro-CT) and high-resolution Nomarski DIC imaging, the current study sought to provide a detailed description of the annular disruptions caused by elevated nuclear pressures within ovine lumbar discs.

■ **Materials and Methods**

Skeletally mature ovine lumbar spines, aged 3 to 5 years, were harvested fresh, wrapped in plastic film, and stored at -20°C for no more than 3 months. In preparation for testing, each lumbar spine was bathed for 2 minutes in room temperature water to aid in the careful removal of all extraneous soft tissues while the spine continued to thaw. A single cut was made along the length of the spine, through the coronal plane of the vertebral foramen, effectively removing all posterior elements, except a small portion of the facet joints (Figure 1B). No attempt was made to remove the residual facet elements for fear of damaging the disc. The spinal cord was removed from the vertebral foramen, whereas the posterior longitudinal ligament was left undisturbed. Three individual vertebra-disc-vertebra motion segments, with all vertebral endplates intact, were isolated from each lumbar spine. Before testing, each motion segment was

soaked for 20 hours in 0.15 M saline at 4°C to ensure a consistent level of hydration.

Following the method of Schechtman *et al*,³⁶ the inferior vertebra of each motion segment was fitted longitudinally with a self-tapping injection screw (major thread diameter, 4.5 mm; internal bore diameter, 1.5 mm), positioned so that its tip was in contact with the center of the nucleus (Figure 1). Through this screw, a hydrated silica gel, thickened with carrageenan, and made radio-opaque by the addition of barium sulfate (25.9% by weight), was injected into the nucleus from a piston-cylinder device that was manually actuated. Motion segments remained unconstrained during the injection process as nuclear pressurization was previously found not to cause a longitudinal expansion of specimens.³⁶

The pressure within the nucleus was gradually increased in a ramp-and-hold manner by repeatedly slowly advancing the piston 0.3 mm at a rate of 0.010 to 0.016 mm/s and then waiting 12 to 14 seconds before the next advance. Nuclear gel injection was continued in this manner until failure of the motion segment occurred, which was marked by a sharp discontinuity in the pressure-time response combined with a large drop in nuclear pressure and often an audible cracking or fibrous tearing. During testing, the pressure of the injected gel was monitored using a pressure transducer (model LM/2345-6, Sensotec, USA; infinite resolution, ±0.3 MPa accuracy) positioned at the base of the injection screw, and recorded at a rate of 2 Hz, using a data acquisition system (data logger model TC-08, PicoLog software version 5.13.4; Pico Technology, UK).

After testing, motion segments were frozen at -20°C and the vertebrae of each segment cut transversely to leave approximately 5 mm of bone attached to both ends of the disc. The radio-opaque gel content of each disc was then digitally captured at a resolution of 34.6 μm, using a micro-CT scanner (model 1172, SkyScan, Belgium) operating at 100 kV/100 μA, then digitally isolated and reconstructed into a 3D image, using a CTAn software (version 1.5.0.2, SkyScan).

Cryosections of the disc, approximately 30 μm in thickness, were obtained using a freezing-sledging microtome. Each disc was sectioned using 1 of 2 methods. The first method involved removing an annular block from the anterior, lateral, posterolateral, and posterior locations of each sagittal half of the disc (Figure 2A). The second method involved dividing each disc and its attached endplates into 5 blocks, 2 from the anterior half of the disc and 3 from the posterior (Figure 2B). Each block was then fixed in 10% formalin (with cetylpyridium chloride), and decalcified in 10% formic acid, allowing full bone-disc-

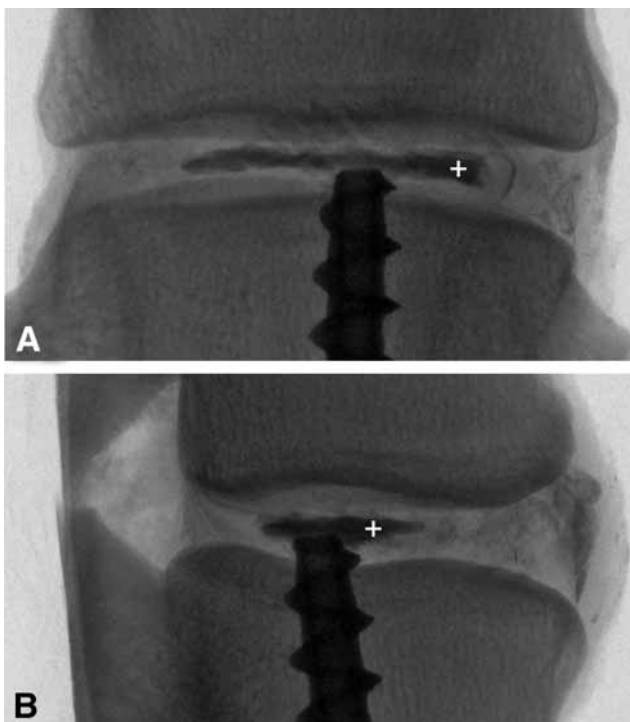


Figure 1. Anterior (A) and lateral (B) radiographs show the central placement of the injection screw tip within the nucleus of a motion segment after testing. The injected contrast-laden gel (+) appears as a dark mass within the center of the disc.

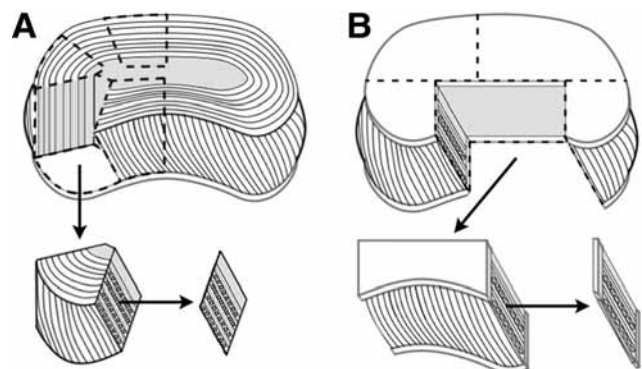


Figure 2. Interlamellar cryosections were collected from unfixed annulus alone (A), or from the annulus with its vertebral endplates still attached after fixation and decalcification (B).

Table 1. Nuclear Pressurization Failure Data for Mature Ovine Lumbar Motion Segments

Lumbar Level	Spine	Failure Pressure (MPa)	Site of Gel Extrusion	Disc Gel Content (mL)
L6–L7	2	12.6	PA/PLA	0.32
L5–L6	1	11.3	PA	0.14
L5–L6	3	12.4	PA	0.12
L5–L6	4	12.0	PA/PLA	0.08
L4–L5	2	14.8	PA	0.24
L3–L4	3	17.2	PA	0.09
L3–L4	4	12.1	PA/PLA	0.13
L2–L3	2	11.3	IV	0.10
L1–L2	3	23.3	IV	0.05
Mean \pm SD		14.1 \pm 3.9		0.14 \pm 0.09

PA indicates posterior annulus; PLA, posterolateral annulus; IV, inferior vertebra.

bone cyrosections to be taken. In each of the 2 methods, cryosections were taken along one of the obliquely oriented annular fiber directions (Figure 2A, B). These sections extended radially from the disc periphery to the nucleus. Detailed investigation of the resulting disruption to the annulus was performed using DIC microscopy to permit structural imaging of the tissue slices in their unstained, fully hydrated state. DIC images of sequential serial slices of the disc annulus were correlated with the 3D micro-CT images of the radio-opaque gel permitting reconstruction of the 3D patterns of annular failure.

■ Results

General Failure Modes. Testing and subsequent inspection of lumbar motion segments were carried out until a repeatable mode of microstructural failure was con-

firmed. In total, 12 motion segments were used for this study, dissected from 4 lumbar spines. Three of the 12 motion segments tested were excluded from the results due to improper placement of injection screw, resulting in pressurization of the inferior vertebra rather than the nucleus. These samples were easily identifiable, marked by both an atypical pressure-time response and micro-CT scan. Mean failure pressure of the remaining 9 motion segments was 14.1 ± 3.9 MPa. Peak rates of pressurization ranged from 0.1 to 0.4 MPa/sec. On failure, 7 of these 9 motion segments extruded gel from the outer annular wall, most commonly from the posterior annulus. The remaining 2 motion segments extruded gel from the inferior vertebra, indicating that rupture of the inferior endplate had occurred. The failure pressure, site of gel extrusion, and volume of gel injected into each successfully pressurized disc are listed in Table 1.

Herniated Samples. For clear interpretation of the included figures, 2 points should be noted. First, the micro-CT images show only the positive image of the radio-opaque gel entrapped within a disc, not the disc structure itself, akin to the images generated using CT-discography in clinical practice. Second, in all microscope images, the injected gel appears black due to its high opacity compared to the disc tissue. Tissue voids with blackened margins in the microscopic images represent the negative image of the injected gel.

From the site of injection, micro-CT images showed that the gel most often spread laterally, filling the nuclear lobes (sites N in Figures 3A, B). In all cases, penetration

Figure 3. Three-dimensional micro-CT gel positive images show only the injected radio-opaque gel entrapped within the disc. Images of 2 typical samples are shown. **A:** superior view of disc L4–L5, spine 2; **B, C:** superior and anterolateral-superior views, respectively, of disc L5–L6, spine 1. A faded image of the vertebral endplate from disc L4–L5, spine 2, has been shown for reference in **A**. N indicates gel within the nucleus; IA, gel penetration of the inner anterior annulus; IP, gel penetration of the inner posterior annulus; IL, gel penetration of the inner lateral annulus; F, gel contained within a fiber bundle; L, gel contained within numerous fiber bundles of a lamella; *, site of gel extrusion. Dashed lines bound triangular regions of severe posterior disruption. Note the lack of a left lateral gel connection (†) in **B**, and **C**; + and ++ mark equivalent locations in these 2 images.

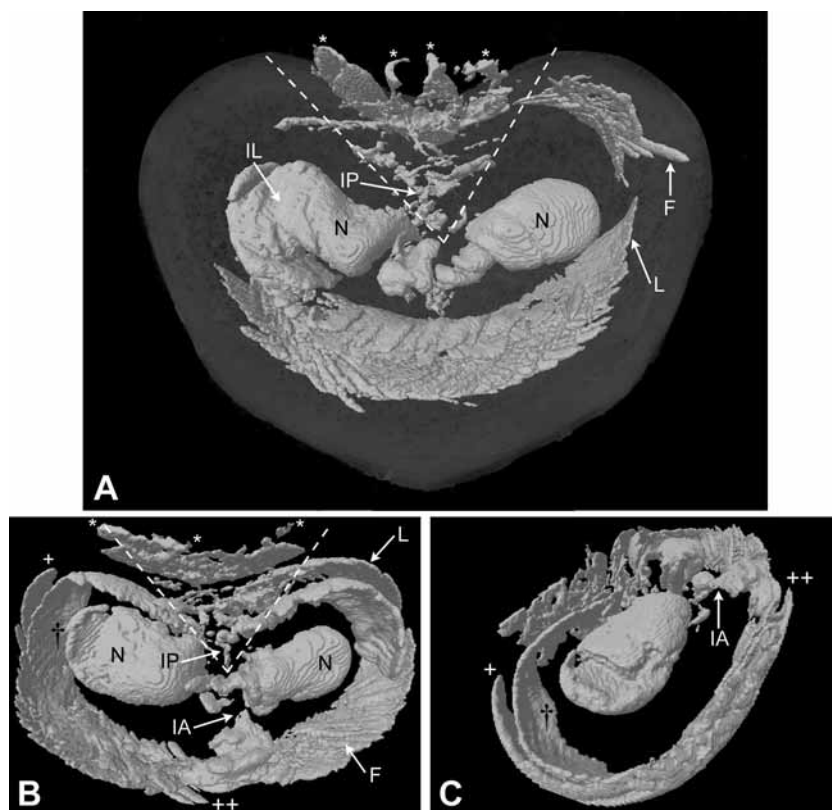
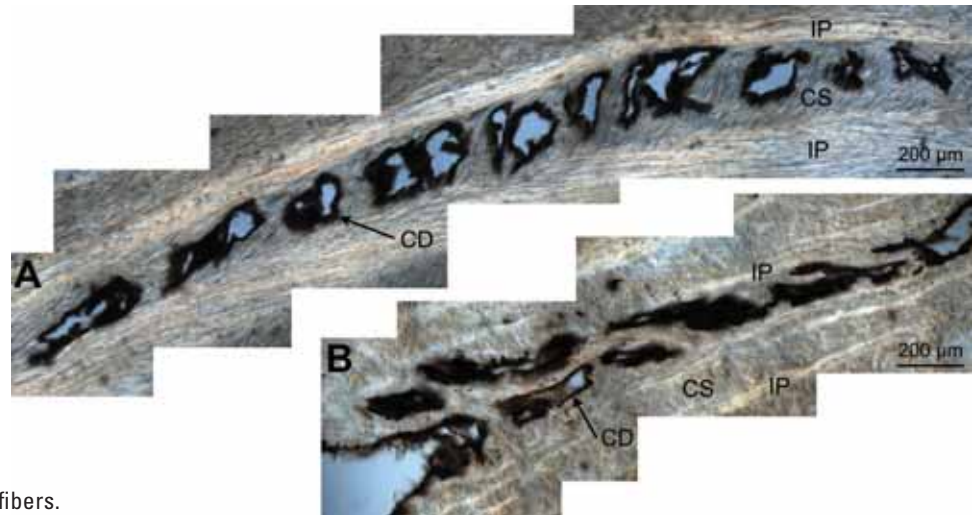


Figure 4. Numerous discrete disruptions (CD) were commonly observed among the cross-sectioned fibers (CS) of lamelle in the mid annulus (A). After sectioning, the highly disrupted annular tissue contained in the center of these disruptions has dispersed into the postsectioning saline creating voids. In essence, image A, is a cross-sectional negative of feature L on the three-dimensional micro-CT gel positive image in Figure 3A or B. Although considerably less often, discrete cross-sectioned disruptions were also found in the inner annulus (B). IP indicates in-plane fibers.



of the inner annulus occurred in the central posterior location (site IP in Figure 3A, B). However, in 5 discs, this was complemented by penetration of additional aspects of the inner annulus, including the central anterior (site IA in Figures 3B, C), lateral (site IL in Figure 3A), and posterolateral regions.

The 3D micro-CT images of the injected gel showed that after penetration of the annulus, it spread circumferentially forming 2 or 3 thin sheets, that followed the lamellae contours (Figure 3A–C). DIC microscopy revealed that each sheet was formed by gel flow within and along the length of numerous consecutive fiber bundles of an individual lamella (Figures 3A, B; Figure 4A). Despite their less distinct structure, even the fibers of the innermost annular lamellae were able to direct the injected gel into discrete flow paths (Figure 4B). Disruption to fiber bundles varied in severity, ranging from minor damage to a small portion of each fiber bundle through to full disruption of entire fiber bundles, including rupture of the bridging elements, which both compartmentalize the fiber bundles of a lamella, and join its 2 neighboring lamellae (Figures 5A–D).³⁴

This pattern of disruption was common to all regions of the annulus except the posterior. In each disc, including those that extruded gel from the posterolateral aspect, gel had disrupted nearly all of the lamellae making up the posterior annulus. Furthermore, gel had not spread circumferentially within the majority of these disrupted lamellae. Instead, it was largely contained within a triangular region oriented with its apex in the central nucleus, and bounded by the posterior/posterolateral junctions (dashed lines in Figure 3A, B). Included in the minority of cases where gel had spread circumferentially from the posterior annulus were the 3 discs that extruded gel from the posterolateral annulus on failure (Table 1). In each of these 3 cases, the posterolateral annulus was largely undisturbed; gel that had reached the outer posterior annulus had tracked circumferentially to the posterolateral aspect where it then breached the outer annular wall.

Within the posterior annulus, the mode of gel disruption was dependent on radial location, *i.e.*, inner or outer annulus. In a similar flow pattern to that observed in the anterior, lateral, and posterolateral annulus, gel flow within the inner and mid posterior annulus occurred predominantly within annular fiber bundles (sites PD in Figure 6B; sites CD and PD in Figure 7). This mode of disruption changed dramatically in the outer annulus where gel had not flowed within lamellae, but between them severing the interlamellar connections (sites BD in Figures 6C, 7). In many cases, the separation of 2 adjacent lamellae extended along the full length of the outer annular fibers from endplate to endplate.

The pattern of lamellar disruption observed in disc L6–L7, spine 2, (Table 1) differed from those in all other discs tested. The 3D micro-CT image of the gel penetration within this disc was largely consistent with those in other samples: gel had spread laterally filling the nuclear lobes, formed sheets following the lamellae contours, and had disrupted nearly all of the lamellae in the posterior annulus. However, microscopic investigation showed that gel-induced disruption had occurred between lamellae in all regions of this disc.

In 5 of the 7 discs that experienced annular failure, radial ruptures within the posterior annulus did not propagate in a straight line from the nucleus to the outer annular wall, but were distributed circumferentially. These ruptures occurred near the mid-axial plane of the disc and were most severe in the outer annulus (Figure 7). Serial sections were required to locate radial ruptures, which were identified by either a sharp change in gel flow path from the radial direction to along the in-plane fiber direction (site Ei in Figure 7B), or as a radially displaced section of lamella (site Em in Figure 7B).

In 2 discs, a single radial rupture extended from the nucleus to outer annulus in a direct path. In the case of disc L3–L4, spine 3, the radial gel rupture path was clearly visible in the micro-CT gel image, which showed an uncharacteristic absence of gel diffusion into the surrounding annular fibers (RP in Figure 8). Inspection of

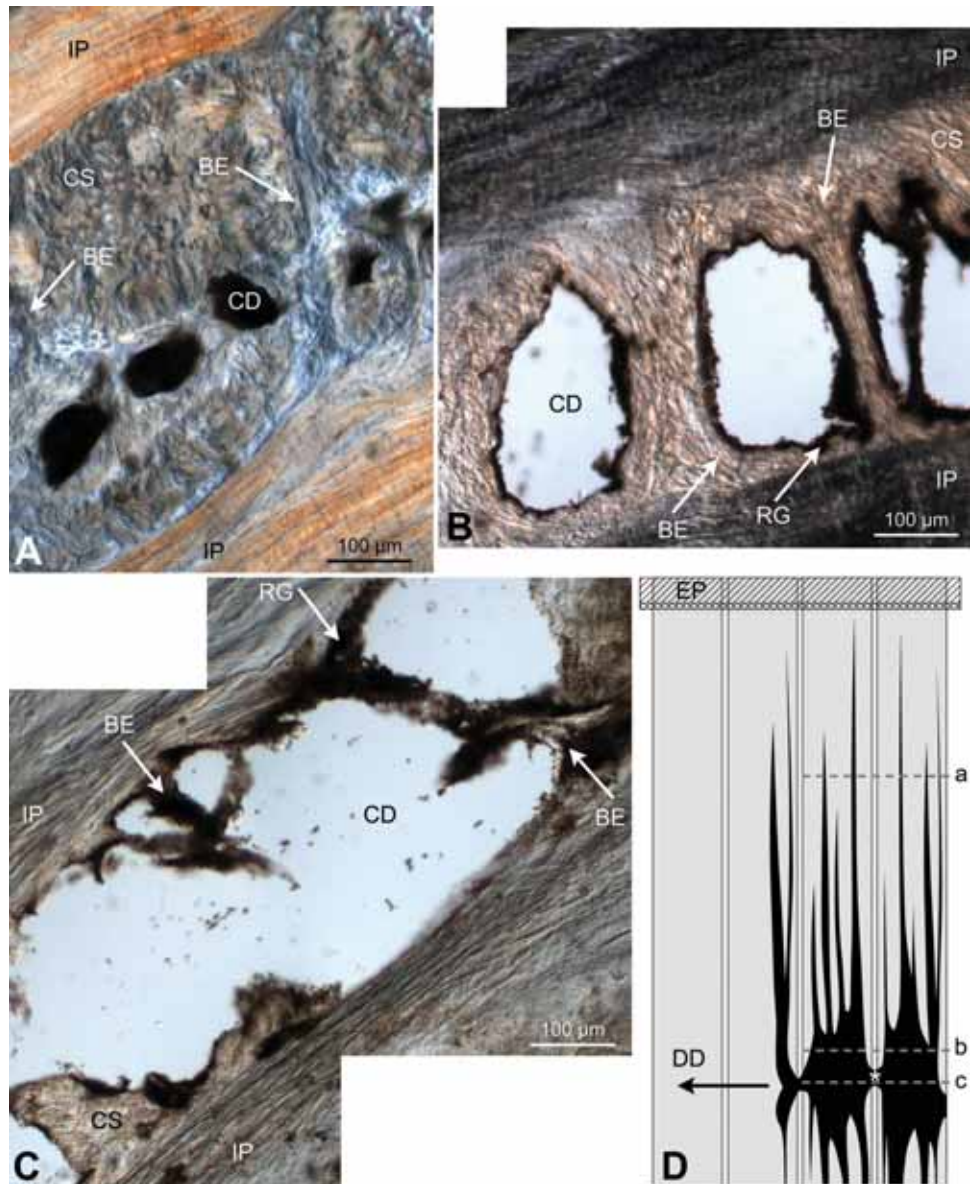


Figure 5. The scope of disruption severity to fiber bundles of a single lamella. The cross-sectioned fiber disruptions (CD) in images **A**, **B**, and **C**, correspond to cross-sectional views of the disrupted annular fiber bundles in schematic **D**, at cutting planes a, b, and c, respectively. Schematic **D**, depicts 4 fiber bundles of a single lamella running in the plane of the page; gel is shown in black. With increasing proximity to the bundle-bundle gel connections (location * in **D**), disruption severity to the fiber bundles increases, culminating in complete destruction of bundles and their bounding bridging elements (BE) (**C**). IP indicates in-plane fibers; CS, cross-sectioned fibers; RG, residual gel; DD, direction of disruption propagation between fiber bundles; EP; endplate.

serial bone-disc-bone sections taken from the posterior annulus showed that this rupture occurred along the superior annulus-endplate junction in the inner annulus (flat region on top of path RP in Figure 8B), and then moved downwards, continuing through the mid and outer annulus near the mid-axial plane (Figure 8C). The other direct radial rupture occurred in disc L3–L4, spine 4, and appears to have initiated from a crack within the cortical endplate near the injection screw, which was probably caused during the screw’s insertion. Serial bone-disc-bone sections showed that this crack was pressurized, eventually causing the overlying portion of cortical bone to break free. Near the start of the mid annulus, the gel exited this crack (site T in Figure 9) and moved upwards to the mid-axial plane, where it proceeded to rupture through the mid and outer annular lamellae (site RL in Figure 9). Interestingly, the rupture path contained a large fragment of cortical endplate lodged in the mid annulus, and a fragment of cartilagi-

nous endplate lodged near the disc periphery (site LF and SF in Figure 9, respectively).

■ Discussion

It is well documented that when loaded in pure compression, the elevated pressure generated within the nucleus of a motion segment causes vertebral end-plate failure before macroscopically visible annular damage.^{37,38} However, compression, and hence elevated hydrostatic nuclear pressures, are thought to play an important role in the development of disc herniation^{15,19,24,26,28,30} and, due to its close morphologic connection,¹¹ possibly internal disc disruption. To study the role that elevated nuclear pressures play in annular disruption, isolated from any other compounding mechanical loads, it is necessary to create a nonphysiologic disruption.

In this study, we have induced annular disruption caused by hydrostatic pressure alone. The use of the nuclear pressurization technique developed by Schechtman

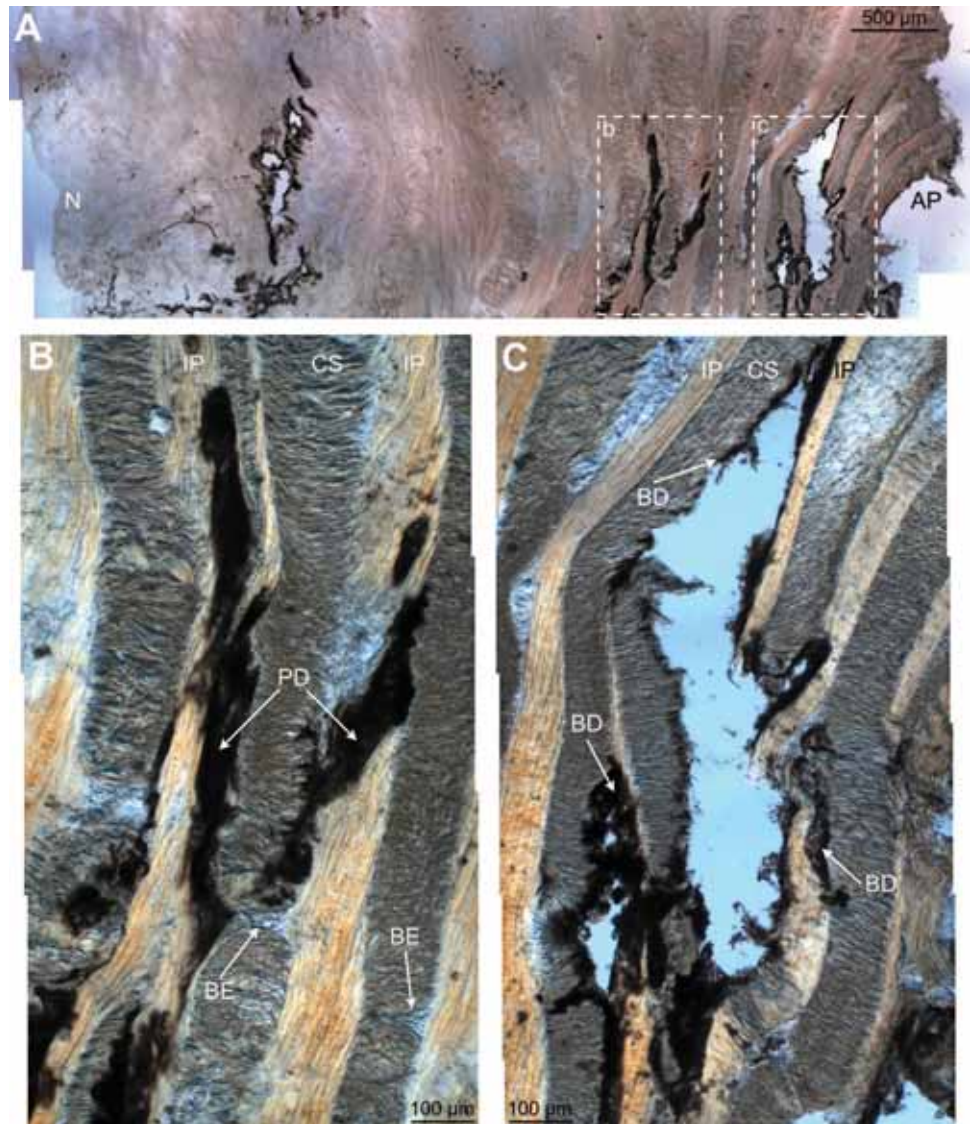


Figure 6. Images from a posterior section of annulus (A) show the change from intralamellar disruption (PD) commonly observed in the mid annulus (B), to interlamellar disruption (BD), which was largely confined to the outer posterior annulus (C). The intralamellar damage shown in B, occurs among in-plane fibers (IP), and is equivalent to a longitudinal view of the intralamellar disruption to cross-sectioned fibers shown at locations CD in Figures 4 and 5. AP indicates the annular periphery; N, nucleus; CS, cross-sectioned fibers; BE, bridging elements.

*et al*³⁶ has allowed direct modulation of the lumbar disc's hydrostatic nuclear pressure without causing any artificial disruption to the annular wall. The introduction of a radio-opaque injection gel has allowed 3D inspection of the resulting disruption, using micro-CT before sectioning and high-resolution inspection *via* DIC microscopy. The use of these investigative techniques in tandem has uncovered several structural features of clinical relevance.

This study clearly demonstrates that the posterior annulus is more vulnerable to structural failure in the presence of hydrostatic loading than any other region of the annulus, even when loaded in a neutral posture. A feature common to all samples was a concentration of severe damage within the posterior annulus, contained within the posterior-posterolateral boundaries (Figure 3A, B). The limited ability of the injected gel to cross these boundaries, effectively concentrating hydrostatic stress within the posterior annulus, indicates that the laminate architecture along these radial lines is of mechanical significance. A concentration of hydrostatic

stress in the posterior annulus is consistent with the clinical observation that the majority of radial fissures and herniation-related ruptures are found within the central or para-central posterior annulus.^{16,35,39} It remains unclear why this distinct pattern of failure occurs in the posterior annulus. However, the low annular wall thickness at this site, and the relatively large number of incomplete lamellae in the adjacent posterolateral annulus are the likely contributing factors.⁴⁰

All regions of the mid annulus, other than the posterior, had the ability to distribute hydrostatic forces circumferentially, creating discrete sheets of disruption that followed the lamellae contours (Figure 3), similar in gross appearance to those created by Oliphant *et al*.⁴¹ These discrete circumferential disruptions were created by gel flow within the numerous fiber bundles of a single lamella (Figures 3, 4A, 5), a disruption mode also observed by Pezowicz *et al*,⁴² and not by the separation of lamellae. This indicates that within the mid annulus, rupturing intralamellar bridging elements between fiber bundles requires significantly less force than is required

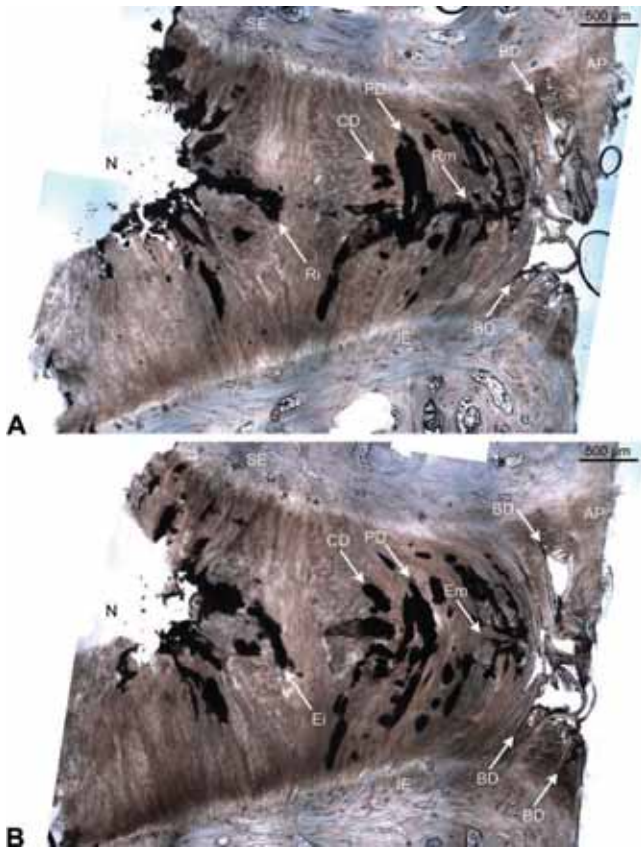


Figure 7. **A**, an image of the posterior annulus shows 2 mid-axial radial ruptures, 1 within the inner annulus (Ri) and a second in the mid annulus (Rm). **B**, a sequential tissue section, separated by approximately 40 [micro]m in the plane of the page from **A**, shows clear evidence of these ruptures (Ei and Em). Cross-sectioned fiber disruptions (CD) and in-plane fiber disruptions (PD) are orthogonal sectional views of gel flow within a fiber bundle (feature F, Figure 3A or B). Note the change from intralamellar disruption (CD and PD) in the inner and mid annulus to interlamellar disruption (BD) in the outer annulus. AP indicates annular periphery; N, nucleus; SE, superior endplate; IE, inferior endplate.

to rupture interlamellar connections. It is therefore possible that a portion of the commonly reported circumferential tears to the mid annulus of degenerate discs^{35,39,43} may actually be created by separation within a lamella, rather than between lamellae.

The abrupt change in disruption pattern from within lamellae in the mid annulus, to between lamellae in the outer posterior annulus clearly demonstrates that these outer lamellae have a distinct lack of interlamellar connectivity (sites PD and CD *vs.* BD in Figures 6, 7). This is even more surprising and significant when one considers that the gel pressure near the disc periphery would certainly be less than the measured nuclear pressure due to frictional resistance encountered along the flow path. From the current results, it is not possible to determine whether this structural distinction is common to all outer lamellae, because disruption to the outer lamellae only occurred frequently in the posterior annulus. This finding suggests that nuclear material migrating down a radial fissure may easily track circumferentially within an

interlamellar space on reaching the inner lamellae of the outer annulus. This may explain why a vast majority of herniations are limited to asymptomatic protrusions^{12,13} and may not develop into an extrusion or sequestration over time.⁴⁴ Furthermore, this finding provides an explanation for the existence of grade 4 internal disc disruption,^{5,9} and additionally supports the proposition made by Osti *et al*³⁹ that such tears are likely caused by mechanical stress.

Radial ruptures from one lamella to the next were always found in the mid-axial plane (sites Ri, Ei, Rm, Em in Figure 7). The natural tendency for fibers to rupture in this location is further illustrated by disc L3–L4, spine 4, where the radial rupture, artificially initiated at the endplate, naturally migrated upwards, continuing through the mid and outer annulus in the mid-axial plane (Figure 9). These observations suggest that for a radial fissure or herniation to occur at the annular-endplate junction, a compounding bending or torsional load is required, consistent with the findings of Adams *et al*²⁴ and Lu *et al*.⁴⁵ Clinically, extruded disc material often contains fragments of cartilaginous endplate.⁴⁶ Although an annular-endplate rupture provides an obvious explanation for this, disc L3–L4, spine 4, demonstrates that if a detached endplate fragment exists within a disc, it could conceivably be swept up and extruded out through a herniation pathway in the mid-axial plane (site SF in Figure 9).

The atypical failures that occurred in disc L6–L7, spine 2, and disc L3–L4, spine 3, suggest that these 2 discs may have possessed inherent annular defects. Disc degeneration and herniation studies carried out on twin populations indicate that some discs are inherently predisposed to structural failure.^{17,18} Spine 2, disc L6–L7, certainly appears to have possessed an inherent lack of interlamellar connection, precipitating widespread interlamellar disruption without any trace of the intralamellar disruptions typically seen. *In vivo*, a disc created with inherently weak interlamellar cohesion would likely experience accelerated delamination, and therefore circumferential cleft formation.³⁵ The only natural annulus-endplate rupture that occurred was in spine 3, disc L3–L4, suggesting that this disc had an inherent lack of structural integrity at this location. Moreover, the lack of gel diffusion into the annular fibers surrounding the radial rupture path suggests that the posterior lamellae gave way suddenly, allowing the gel to reach the periphery of the disc very quickly (Figure 8). Interestingly, the failure pressures of these 2 aforementioned samples were consistent with the observed mean. However, their disruption patterns suggest that they possessed an inherent, but as yet unidentifiable, fine-scale difference in annular architecture.

In the current study, the sample size was determined based on the authors' ability to clearly identify a repeatable mode of microstructural failure. This was possible

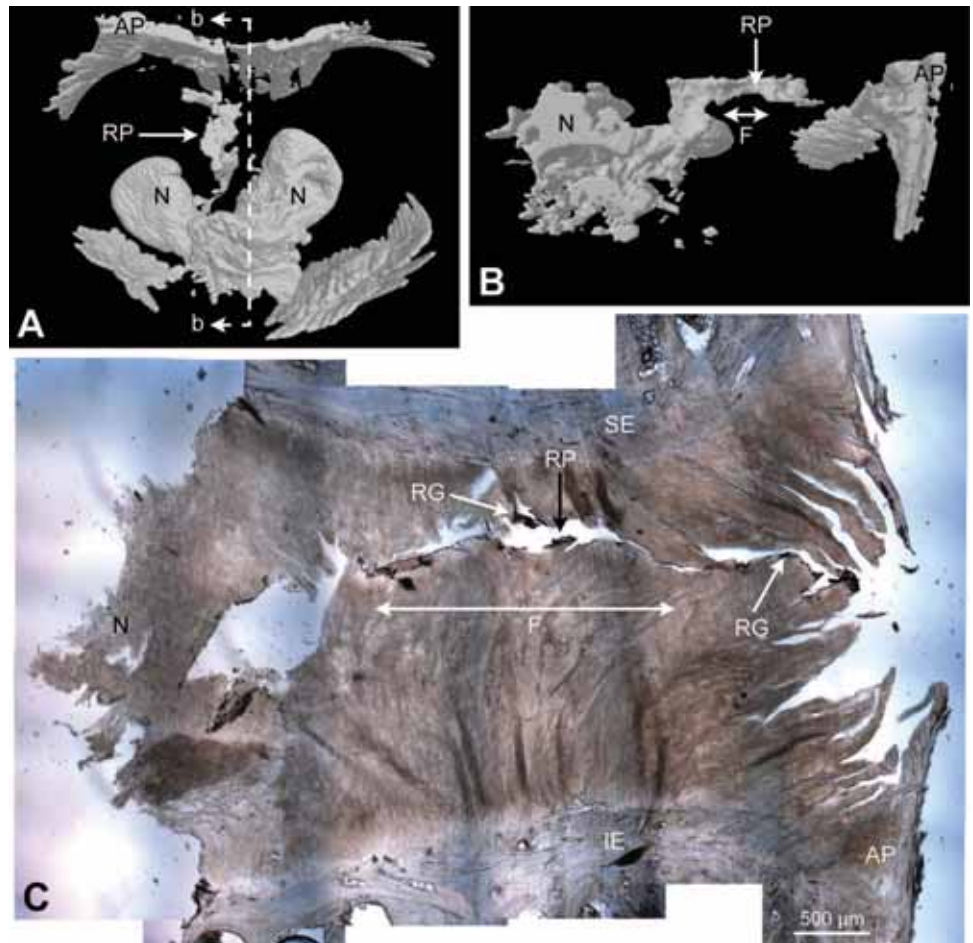


Figure 8. Superior (A) and lateral (B) micro-CT gel positive images show a direct gel rupture path (RP) from the nucleus (N) to the annular periphery (AP). C, shows the gel negative image of this same rupture path (feature F common to images C, and B) and confirms the absence of gel diffusion into the surrounding annulus. SE indicates superior endplate; IE, inferior endplate; RG, residual gel.

after testing and inspecting 12 motion segments due to the consistent features displayed by the herniated discs. However, it is certainly probable that given a larger sample size, a more defined spectrum of less typical failure characteristics could have been reported. The relatively small sample size employed in this study should therefore be recognized as a limitation.

The ovine lumbar disc was selected for this study over other potential animal models for 2 reasons. First, a consistent, reliable supply of fully intact ovine lumbar spines was available for this and future studies. Second, the ovine lumbar disc is comparable to the human lumbar disc in biochemical composition,⁴⁷ gross anatomic structure,⁴⁸ and biomechanical function.^{49,50} Despite these similarities, it must be noted that no formal interspecies comparison of the disc's laminate characteristics, such as the number of distinct lamellae, incomplete lamellae, and lamella thickness, has been conducted. Care should therefore be taken in interpreting the results outlined above.

The use of nondegenerate human lumbar discs for this study would have been impractical. Substantial age-related changes in the human lumbar disc annulus begin in the second decade of life⁵¹; therefore, young tissue would have been required, which is highly problematic to obtain due to the ethical processes required. Furthermore, annular defects such as rim lesions and cir-

cumferential tears that do not connect to the nucleus are not detectable using CT-discography. Thus, even if suitable human tissue could be obtained, a blank canvas on which to paint a biomechanically sensitive detailed structural investigation such as this could not be guaranteed. Although it could be argued that this equally applies for sheep, there is no doubt that the range of environmental factors to which sheep are exposed is much more limited, and uniform, than that for a human population.

■ Conclusion

The posterior-posterolateral annular boundary is of significant mechanical importance, and serves to concentrate hydrostatic stress within the posterior annulus, leading to a distinct pattern of annular failure. This finding provides clear rationale for why both radial ruptures and herniations are predominantly found in the posterior annulus.

Within the mid annulus, the predominance of disruptions within lamellae show that interlamellar connections are stronger than the intralamellar portion of bridging elements, that separate fiber bundles. This suggests that some of the circumferential tears to the mid annulus observed clinically may actually be caused by the destruction of a lamella, rather than failure of the interlamellar connections.



Figure 9. Annular failure in association with endplate disruption. A direct gel rupture path was artificially initiated by a fracture in the inferior vertebral endplate (IE) along edge UE. From the terminus of the endplate fracture (T) the gel rupture continues through the mid and outer annulus in the mid-axial plane. As a result of the endplate disruption, a large fragment of bone (LF) was lodged in the mid annulus, and more interestingly, a smaller fragment of cartilaginous endplate (SF) was carried to the annular periphery (AP), towing attached lamellae with it (RL). N indicates nucleus; SE, superior endplate.

Weak interlamellar connections are characteristic of the outer posterior annulus, consistent with the observation that interlamellar concentric tears often occur in this location. This finding suggests that such tears are caused primarily by mechanical factors rather than degenerative effects.

Radial rupture paths created by hydrostatic pressure alone occur in the mid-axial plane, indicating that a compounding mechanical load is required in order to cause a rupture at the annulus-endplate junction.

Finally, the finding of a limited number of highly atypical annular failures agrees well with the notion that some discs contain inherent annular defects, predisposing them to failure by mechanical forces.

■ Key Points

- With respect to the annular wall, the posterior region is most susceptible to failure in the presence of high nuclear pressure, even when loaded in the neutral position.
- Within the mid annulus, intralamellar bridging elements separating annular fiber bundles fail before interlamellar connections.
- The lamellae of the outer posterior annulus possess weaker interlamellar cohesion than those of the mid annulus.

- Radial ruptures of the annulus due to hydrostatic pressure alone occur in the mid-axial plane.
- Discs may contain inherent structural features that predispose the discs to a certain mode of annular disruption.

Acknowledgments

The authors are grateful for the award of grants in support of this research from both the NZ Orthopedic Association Wishbone Trust and Medtronic Australasia.

References

1. Bogduk N, Tynan W, Wilson AS. The nerve supply to the human lumbar intervertebral discs. *J Anat* 1981;132:39–56.
2. Palmgren T, Grönblad M, Virri J, et al. An immunohistochemical study of nerve structures in the annulus fibrosus of human normal lumbar intervertebral discs. *Spine* 1999;24:2075–9.
3. Rooft PG. Innervation of annulus fibrosus and posterior longitudinal ligament. *Arch Neurol Psychiatry* 1940;44:110–13.
4. Kuslich SD, Ulstrom CL, Michael CJ. The tissue origin of low back pain and sciatica. *Orthop Clin North Am* 1991;22:181–7.
5. Aprill C, Bogduk N. High-intensity zone: a diagnostic sign of painful lumbar disc on magnetic resonance imaging. *Br J Radiol* 1992;65:361–9.
6. Moneta GB, Videman T, Kaivanto K, et al. Reported pain during lumbar discography as a function of annular ruptures and disc degeneration. A re-analysis of 833 discograms. *Spine* 1994;19:1968–74.
7. Vanharanta H, Sachs BL, Spivey M, et al. A comparison of CT/discography, pain response and radiographic disc height. *Spine* 1988;13:321–4.
8. Crock HV. A reappraisal of intervertebral disc lesions. *Med J Aust* 1970;1:983–9.

9. Schwarzer AC, Aprill CN, Derby R, et al. The prevalence and clinical features of internal disc disruption in patients with chronic low back pain. *Spine* 1995;20:1878–83.
10. Adams MA, Bogduk N, Burton K, et al. *The Biomechanics of Back Pain*. London: Churchill Livingstone; 2002.
11. Bogduk N. *Clinical Anatomy of the Lumbar Spine and Sacrum*. 4th ed. London: Elsevier Churchill Livingstone; 2005.
12. Boden SD, Davis DO, Dina TS, et al. Abnormal magnetic-resonance scans of the lumbar spine in asymptomatic subjects. A prospective investigation. *J Bone Joint Surg Am* 1990;72:403–8.
13. Jensen MC, Brant-Zawadzki MN, Obuchowski N, et al. Magnetic resonance imaging of the lumbar spine in people without back pain. *N Engl J Med* 1994;331:69–73.
14. Weishaupt D, Zanetti M, Hodler J, et al. MR imaging of the lumbar spine: prevalence of intervertebral disk extrusion and sequestration, nerve root compression, end plate abnormalities, and osteoarthritis of the facet joints in asymptomatic volunteers. *Radiology* 1998;209:661–6.
15. Boos N, Rieder R, Schade V, et al. The diagnostic accuracy of magnetic resonance imaging, work perception, and psychosocial factors in identifying symptomatic disc herniations. *Spine* 1995;20:2613–25.
16. Maezawa S, Muro T. Pain provocation at lumbar discography as analyzed by computed tomography/discography. *Spine* 1992;17:1309–15.
17. Battié MC, Videman T, Gibbons LE, et al. Determinants of lumbar disc degeneration. A study relating lifetime exposures and magnetic resonance imaging findings in identical twins. *Spine* 1995;20:2601–12.
18. Battié MC, Haynor DR, Fisher LD, et al. Similarities in degenerative findings on magnetic resonance images of the lumbar spines of identical twins. *J Bone Joint Surg Am* 1995;77:1662–70.
19. Kelsey JL, Githens PB, White AA III, et al. An epidemiologic study of lifting and twisting on the job and risk for acute prolapsed lumbar intervertebral disc. *J Orthop Res* 1984;2:61–6.
20. Mundt DJ, Kelsey JL, Golden AL, et al. An epidemiologic study of non-occupational lifting as a risk factor for herniated lumbar intervertebral disc. *Spine* 1993;18:595–602.
21. Fathallah FA, Marras WS, Parnianpour M. The role of complex, simultaneous trunk motions in the risk of occupation-related low back disorders. *Spine* 1998;23:1035–42.
22. Marras WS, Lavender SA, Leurgans SE, et al. The role of dynamic three-dimensional trunk motion in occupationally-related low back disorders. The effects of workplace factors, trunk position, and trunk motion characteristics on risk of injury. *Spine* 1993;18:617–28.
23. Adams MA, Freeman BJ, Morrison HP, et al. Mechanical initiation of intervertebral disc degeneration. *Spine* 2000;25:1625–36.
24. Adams MA, Hutton WC. Prolapsed intervertebral disc. A hyperflexion injury 1981 Volvo Award in Basic Science. *Spine* 1982;7:184–91.
25. Adams MA, Hutton WC. The effect of fatigue on the lumbar intervertebral disc. *J Bone Joint Surg* 1983;65:199–203.
26. Adams MA, Hutton WC. Gradual disc prolapse. *Spine* 1985;10:524–31.
27. Callaghan JP, McGill SM. Intervertebral disc herniation: studies on a porcine model exposed to highly repetitive flexion/extension motion with compressive force. *Clin Biomech* 2001;16:28–37.
28. Gordon SJ, Yang KH, Mayer PJ, et al. Mechanism of disc rupture: a preliminary report. *Spine* 1991;16:450–6.
29. Kuga N, Kawabuchi M. Histology of intervertebral disc protrusion: an experiment study using an aged rat model. *Spine* 2001;26:E379–84.
30. McNally DS, Adams MA, Goodship AE. Can intervertebral disc prolapse be predicted by disc mechanics? *Spine* 1993;18:1525–30.
31. Simunic DI, Broom ND, Robertson PA. Biomechanical factors influencing nuclear disruption of the intervertebral disc. *Spine* 2001;26:1223–30.
32. Simunic DI, Robertson PA, Broom ND. Mechanically induced disruption of the healthy bovine intervertebral disc. *Spine* 2004;29:972–8.
33. Pezowicz CA, Robertson PA, Broom ND. Intralamellar relationships within the collagenous architecture of the annulus fibrosus imaged in its fully hydrated state. *J Anat* 2005;207:299–312.
34. Pezowicz CA, Robertson PA, Broom ND. The structural basis of interlamellar cohesion in the intervertebral disc wall. *J Anat* 2006;208:317–30.
35. Vernon-Roberts B, Fazzalari NL, Manthey BA. Pathogenesis of tears of the annulus investigated by multiple-level transaxial analysis of the T12–L1 disc. *Spine* 1997;22:2641–6.
36. Schechtman H, Robertson PA, Broom ND. Failure strength of the bovine caudal disc under internal hydrostatic pressure. *J Biomech* 2006;39:1401–9.
37. Roaf R. A study of the mechanics of spinal injuries. *J Bone Joint Surg* 1960;42:810–23.
38. Yoganandan N, Maiman DJ, Pintar F, et al. Microtrauma in the lumbar spine: a cause of low back pain. *Neurosurgery* 1988;23:162–8.
39. Osti OL, Vernon-Roberts B, Moore R, et al. Annular tears and disc degeneration in the lumbar spine. A post-mortem study of 135 discs. *J Bone Joint Surg Br* 1992;74:678–82.
40. Marchand F, Ahmed AM. Investigation of the laminate structure of lumbar disc annulus fibrosus. *Spine* 1990;15:402–10.
41. Oliphant D, Frayne R, Kawchuk G. A new method of creating intervertebral disc disruption of various grades. *Clin Biomech* 2006;21:21–5.
42. Pezowicz CA, Schechtman H, Robertson PA, et al. Mechanisms of annular failure resulting from excessive intradiscal pressure: a microstructural-micromechanical investigation. *Spine* 2006;31:2891–903.
43. Vernon-Roberts B, Pirie CJ. Degenerative changes in the intervertebral discs of the lumbar spine and their sequelae. *Rheumatol Rehabil* 1977;16:13–21.
44. Boos N, Semmer N, Elfering A, et al. Natural history of individuals with asymptomatic disc abnormalities in magnetic resonance imaging: predictors of low back pain-related medical consultation and work incapacity. *Spine* 2000;25:1484–92.
45. Lu YM, Hutton WC, Gharpuray VM. Do bending, twisting, and diurnal fluid changes in the disc affect the propensity to prolapse? A viscoelastic finite element model. *Spine* 1996;21:2570–9.
46. Moore RJ, Vernon-Roberts B, Fraser RD, et al. The origin and fate of herniated lumbar intervertebral disc tissue. *Spine* 1996;21:2149–55.
47. Reid JE, Meakin JR, Robins SP, et al. Sheep lumbar intervertebral discs as models for human discs. *Clin Biomech* 2002;17:312–4.
48. Wilke HJ, Kettler A, Wenger KH, et al. Anatomy of the sheep spine and its comparison to the human spine. *Anat Rec* 1997;247:542–55.
49. Wilke HJ, Kettler A, Claes LE. Are sheep spines a valid biomechanical model for human spines? *Spine* 1997;22:2365–74.
50. Smit TH. The use of a quadruped as an in vivo model for the study of the spine - biomechanical considerations. *Eur Spine J* 2002;11:137–44.
51. Boos N, Weissbach S, Rohrbach H, et al. Classification of age-related changes in lumbar intervertebral discs. *Spine* 2002;27:2631–44.